Protein composition of 6K2-induced membrane structures formed during *Potato virus A* infection

Andres Lõhmus[1], Markku Varjosalo[2] and Kristiina Mäkinen[1]*

1. Department of Food and Environmental Sciences, University of Helsinki, Finland
2. Institute of Biotechnology, University of Helsinki, 00014 Helsinki, Finland.

*Corresponding author

Kristiina Mäkinen

Department of Food and Environmental Sciences

P.O.Box 27

00014 University of Helsinki

Finland

e-mail: kristiina.makinen@helsinki.fi

Tel: +358294158411

Keywords: Potato virus A, Potyvirus, 6K2 protein, viral replication complex, proteome

Running head: PVA replication complex proteome

Word count: 6779

Summary

Defining the precise molecular composition of membranous replication compartments is a key to understanding the mechanisms of virus multiplication. Here we set out to investigate the protein composition of the potyviral replication complexes. We purified the potyviral 6K2 protein-induced membranous structures from *Potato virus A* (PVA) infected *Nicotiana benthamiana* plants. For this purpose the 6K2 protein, which is the main inducer of potyviral membrane rearrangements, was expressed in fusion with an N-terminal Twin-Strep-tag and Cerulean fluorescent protein (SC6K) from the infectious PVA cDNA. A non-tagged Cerulean-6K2 (C6K) virus and the SC6K protein alone in the absence of infection were used as controls. A purification scheme exploiting discontinuous sucrose gradient centrifugation followed by Strep-tag-based affinity chromatography was developed. Both (+)- and (-)strand PVA RNA and viral protein VPg were co-purified specifically with the affinity tagged PVA-SC6K. The purified samples, which contained individual vesicles and membrane clusters, were subjected to mass spectrometry analysis. Data analysis revealed that many of the detected viral and host proteins were either significantly enriched or fully specifically present in PVA-SC6K samples when compared to the controls. Eight out of eleven potyviral proteins were identified with high confidence from the purified membrane structures formed during PVA infection. Ribosomal proteins were identified from the 6K2-induced membranes only in the presence of a replicating virus, reinforcing the tight coupling between replication and translation. A substantial number of proteins associating with chloroplasts and several host proteins previously linked with potyvirus replication complexes were co-purified with PVA-derived SC6K, supporting the conclusion that the host proteins identified in this study may have relevance in PVA replication.

Introduction

Positive-strand RNA ((+)RNA) viruses replicate in association with host membranes (Miller and Krijnse-Locker, 2008). This association results in rearrangement of cellular membranes to accommodate viral replication machineries, hide viral RNA and proteins from host defense systems and provide an environment to concentrate host and viral factors for viral RNA (vRNA) synthesis (den Boon and Ahlquist, 2010; Verchot, 2011). Among different groups of (+)RNA viruses the virus-induced membraneous replication complexes vary greatly in their origin, size, and shape (reviewed in Paul and Bartenschlager, 2013). The formation of viral replication complexes (VRCs) in (+)RNA viruses requires an orchestrated assembly of many host and viral proteins (Mine and Okuno, 2012). Host factors involved in viral multiplication represent potential targets for virus control and therefore their identification and functional characterization is important.

The genus *Potyvirus* is economically one of the most devastating groups of plant viruses in the world affecting the production of nearly all cultivated plant species. The genome of potyviruses is a positive-sense single-stranded RNA of approximately 10 kb. Ten out of eleven potyviral proteins are synthesized from a large open reading frame (ORF) whereas the eleventh protein, P3N-PIPO, is produced from a separate partially overlapping ORF (reviewed in Revers and García, 2015). P3N-PIPO expression is enabled by transcriptional slippage, specific for viral RNA polymerase (Olspert *et al.*, 2015; Rodamilans *et al.*, 2015). Formation of potyviral VRCs is initiated at the endoplasmic reticulum (ER) wherefrom the individual VRC vesicles are transported to chloroplasts via the endosomal trafficking pathway aided by the actomyosin system (Wei *et al.*, 2010; Wei and Wang, 2008). As the infection progresses, these vesicles fuse with chloroplasts in a process requiring plant SNARE protein Syp71 (Wei *et al.*, 2013). Finally, late in the infection,

the chloroplast-associated VRCs aggregate into large perinuclear globular structures (Grangeon *et al.*, 2012).

The hydrophobic membrane-associated potyviral protein 6K2 is a multifunctional protein participating in VRC formation, long distance movement and symptom development (Rajamäki and Valkonen, 1999; Spetz and Valkonen, 2004). 6K2 is able to induce vesicle formation at ER membranes even in the absence of infection (Beauchemin *et al.,* 2007; Schaad *et al.,* 1997; Thivierge *et al.,* 2008). Most of the potyviral proteins, including P3, CI, 6K2, VPg, NIapro and NIb, have been shown to associate with 6K2-induced VRCs (Beauchemin *et al.,* 2007; Cotton *et al.,* 2009; Dufresne *et al.,* 2008). The RNA helicase activity of CI (Carrington *et al.*, 1998; Fernández *et al.*, 1997; Kekarainen *et al.*, 2002), the putative role of VPg as a primer for RNA synthesis (Anindya *et al.*, 2005; Puustinen and Mäkinen, 2004; Rantalainen *et al.*, 2011) and the RNA synthesis activity of NIb (Hong and Hunt, 1996) are essential for amplification of viral RNA. Although P3 is also required for replication (Klein *et al.*, 1994), the molecular mechanism how it exerts its replication-associated function is not clear. P3N-PIPO and CP are dispensable for replication (Mahajan *et al.*, 1996; Wen and Hajimorad, 2010).

Host factors have various roles in replication including RNA recruitment, assembly and activation of VRCs, (-)- and (+)strand synthesis activity, asymmetry in (+)strand production and adjustment of the lipid composition (e.g. Barajas *et al.*, 2014; Huang *et al.*, 2012; Wei *et al.*, 2013; reviewed by Nagy and Pogany, 2012 and Wang, 2015). Reconstitution of various replication reactions in yeast extracts supplemented with viral replication proteins has been a powerful tool to study the specific roles of the host proteins in tombusvirus replication (Pogany and Nagy, 2008). Although such an experimental tool is not available to study the replication reactions of potyviruses, a lot of biochemistry and cell biology work has been done to identify host proteins associated with 6K2-induced vesicles. The importance of these

structures for viral replication is emphasized by the presence of double-stranded viral RNA and active vRNA synthesis in *Turnip mosaic virus* (TuMV)-induced vesicles (Cotton *et al.*, 2009).

Paul and colleagues (Paul *et al.*, 2013) used a membrane pull-down approach to study the molecular composition of membranous replication compartments of human *Hepatitis C virus* (HCV; family *Flaviviridae*). They isolated double-membrane vesicles (DMVs) and demonstrated active HCV RNA synthesis in them. Further biochemical and morphological studies revealed the presence of many viral and host proteins in DMVs as well as details of their lipid composition.

We chose a similar approach to study the protein composition of potyviral VRCs. 6K2 protein fused to an affinity tag and Cerulean fluorescent protein (CFP) was used to purify 6K2-induced membrane structures from PVA infected *Nicotiana benthamiana* plants. Although 6K2 appears to be an optimal marker protein for potyviral VRCs, it doesn't readily tolerate modifications in its natural genomic context (Spetz and Valkonen, 2004). To overcome this, an additional copy of 6K2 gene is usually inserted to a different location in the genome. Successful visualization of TuMV VRCs has been achieved using this approach (Cotton *et al.*, 2009; Thivierge *et al.*, 2008; Wei *et al.*, 2010). We inserted the Strep-tagged CFP fused 6K2 protein in between NIb and CP coding regions and purified the membrane structures from infected and non-infected *N. benthamiana* leaves.

Our main goal was to identify the protein composition of the PVA VRCs. To achieve this, we performed a proteomic analysis of the purified 6K2-induced membrane structures. These data produced will facilitate functional studies of the host proteins involved in potyviral replication in future.

Results

Establishment of infectious PVA cDNA encoding Twin-Strep-tagged 6K2

We set out to purify the putative PVA VRCs via the membrane-associated 6K2 protein. To allow visualization of the 6K2-induced structures, we expressed the 6K2 with a fluorescent marker from PVA infectious cDNA (icDNA). PVA-C6K construct allowed the expression of CFP in fusion with the N-terminus and PVA-6KY construct yellow fluorescent protein (YFP) in fusion with the C-terminus of the 6K2 protein (Fig. 1). NIa protease cleavage sites were engineered to flank the 6K2 fusion protein to aid the polyprotein processing.

Agrobacterium infiltration was used to introduce PVA-C6K and PVA-6KY icDNAs into *Nicotiana benthamiana* leaves. Both viruses were spreading approximately with a similar speed (Fig. S1). Next, we studied the infection of PVA-C6K and PVA-6KY by confocal microscopy (Fig. 2a). Scattered individual vesicles and hardly any aggregation with chloroplasts was observed with CFP-6K2 (Fig. 2a left panels) whereas 6K2-YFP -induced vesicles associated predominantly with chloroplasts (Fig. 2a middle panels). The lack of CFP-6K2 chloroplast labeling was a puzzling observation since VRC vesicle fusion with the outer chloroplast membrane is required for replication (Wei *et al.*, 2010). We therefore studied the infection in the systemic leaves by electron microscopy (Fig. 2b). The hallmarks of potyviral infection, cylindrical inclusions, and virus particles were observed in both PVA-C6K- and PVA-6KY-infected cells. We concluded that both viruses, PVA-C6K and PVA-6KY, caused normal infection.

To establish which virus, PVA-C6K or PVA-6KY, should be used for purification, we used GFP-trap purification, which allows isolation of fluorescent fusion proteins. The N-terminally fused CFP gave better yields (Fig. 2c), suggesting that the tag is better

exposed in this orientation, which led us to choose PVA-C6K for the purification of VRCs.

Twin-Strep-tag (hereafter 2xStrep-tag) consists of two copies of an eight amino acids (WSHPQFEK) long peptide, and allows efficient purification of proteins under native conditions (Schmidt and Skerra, 2007). We fused 2xStrep-tag encoding sequence to CFP-6K2 gene in PVA-C6K, thus creating PVA-SC6K icDNA. Systemic infection by PVA-SC6K was confirmed by an immunoblot analysis (Fig. 2d). PVA-C6K was used as a control to verify tag-specific purification of the proteins. In addition, we cloned a membrane control construct (MC-SC6K; Fig. 1) to express monocistronic SC6K from a plant expression vector (mcSC6K). The purpose of MC-SC6K control was to reveal the host proteins associated with 6K2-induced membranous structures in the absence of a replicating virus. Excluding these proteins from the final list should therefore reveal proteins present in the membranous replication structures during infection.

Purification and characterization of membranous 6K2-induced structures from PVA infected cells

To obtain PVA 6K2-induced membranous structures, *Nicotiana benthamiana* plants were *Agrobacterium* infiltrated to initiate PVA-SC6K and PVA-C6K infections and MC-SC6K expression. The systemically infected leaves were collected at 10 days post infiltration (dpi) and leaves transiently expressing mcSC6K at 4 dpi. The purification scheme is depicted in Fig. 3a. The membranous SC6K- and C6K-associated structures were enriched by sucrose gradient centrifugation prior to affinity purification. The presence of C6K or SC6K in the collected fractions was confirmed by Western blotting with an anti-GFP antibody. The Western blot analysis revealed that most of SC6K was concentrated to the fraction five in the virus-infected

samples (Fig. 3b, left panel). In the non-infected mcSC6K expressing sample the signal concentrated to fractions 5-7 (Fig. 3b, right panel). This analysis revealed also the presence of an approximately 27 kDa product, representing free CFP, which explains the cytoplasmic background fluorescence observed in confocal microscopy (see Fig. 2b). Free CFP in the top fractions showed that the SC6K-containing fractions were well separated from those containing soluble cytosolic proteins. The affinity purification of SC6K-containing membranes was carried out on a Strep-Tactin matrix from fractions 5 of each sample. A clear enrichment of SC6K was observed in the PVA-SC6K sample eluate whereas no C6K was detected in the PVA-C6K sample eluate (Fig 3c), indicating efficient tag-specific purification. A clear difference in the total protein content between the purified PVA-SC6K proteins and the controls was detected in the silver-stained gels (Fig 3d). Protein quantification from the purified membranes showed that the PVA-SC6K and MC-SC6K samples contained higher concentration of proteins than the PVA-C6K samples (Fig. S2).

Quantitative RT-PCR showed that PVA RNA copy number was greater in PVA-C6K than in PVA-SC6K input prior to purification and vice versa after purification (Fig. S3), indicating that the yield of PVA RNA was significantly higher from PVA-SC6K sample than from PVA-C6K control. Approximately 5.2% of PVA RNA present in the input was recovered in the PVA-SC6K sample compared to approximately 0.6% in the PVA-C6K control the fold of enrichment being 8.7 (Fig. 4a). RT-PCR with both (+)- and (-)-strand PVA RNA specific primers revealed a strong (+)-strand and a weak (-)-strand specific signal in the PVA-SC6K sample, showing that it contained PVA RNA of both polarities (Fig. 4b). A weak (+)-strand specific signal in the PVA-C6K control sample suggests that some unspecific binding of C6K-containing membranes and / or PVA particles to Strep-tactin matrix took place. Western-blot analysis with VPg antibody revealed tag-specific purification of the essential

replication protein VPg in the PVA-SC6K sample (Fig. 4c). The origin of the high molecular weight signal in the VPg blot is not clear. It may represent polyprotein intermediates, protein complexes that were not fully dissociated during SDS-PAGE or VPg-RNA complexes.

We compared negatively-stained 6K2-membranes from PVA-SC6K infection and from the controls under electron microscopy (EM; Fig. 5). The analysis showed that 2xStrep-tagged samples, from PVA-SC6K infection and mcSC6K expression, contained abundantly vesicles and vesicle clusters (Fig. 5 upper and lower panels) whereas only very few vesicles were present in the control PVA-C6K sample (Fig. 5 middle panels). The sizes of small vesicles purified in all of the samples varied between 40-90 nm, the mean being 56 nm (Fig. 5). EM images from all samples also show elongated membranous structures. Virions were present in both virus samples with no notable difference in their quantity between PVA-SC6K and PVA-C6K materials. This suggests that virions were interacting un-specifically with the Strep-Tactin matrix to some extent (Fig. 5 panels on the right).

LC-MS/MS analysis of the affinity purified membranous 6K2-induced structures

The affinity purified PVA-SC6K samples were subjected to liquid chromatography-tandem mass spectrometry (LC-MS/MS) analysis in three biological replicates together with the corresponding PVA-C6K and MC-SC6K control samples. The MS analysis identified 729 proteins in the PVA-SC6K samples, and 102 in PVA-C6K and 49 in MC-SC6K control samples. All unique proteins identified in these samples are given in Table S1.

The number of peptide spectrum matches (PSMs) in the purified PVA-SC6K vesicle sample was the highest for the bait protein SC6K. Out of 40 identified SC6K-peptides 7 corresponded to 6K2, 4 to 2xStrep and 29 to CFP. The second highest PSM scores were those of the viral proteins CI and HCpro with almost identical PSM scores, 137 and 136, respectively (see Table 1). Both CI and HCpro were identified also from PVA-C6K control sample but had significantly lower PSM scores, 2 and 3, respectively. Therefore, it is clear that both CI and HCpro were purified in a tag-specific manner and are abundantly present in SC6K-induced vesicles during PVA infection. The viral proteins P3, 6K1, VPg, NIa-pro and NIb were detected with high confidence and can be thought to associate genuinely with the 6K2-induced vesicles during infection. The presence of CP is at least partially unspecific. CP's PSM score in the PVA-SC6K sample was 3.6 times higher compared to the PVA-C6K control sample (18 vs 5, respectively). Undoubtedly, virions contributed to the presence of CP in the MS data as EM analysis revealed PVA particles in both PVA-SC6K and PVA-C6K samples (see Fig. 5). One viral P1 protein-specific peptide was found in only one of the three biological replicates. Two N-terminal peptides from P3 could be derived from P3N-PIPO but no peptides matching to the PIPO part were identified.

Next the host proteins identified by LC-MS/MS were sorted in to a list presenting the host proteins which were identified with the highest confidence and fold of enrichment compared to the controls. The final list, presented in Table 2, contains proteins for which peptides were found in at least two biological replicates amounting to at least four peptides, two of them unique. The threshold value for the fold of enrichment calculated from PSM values was set to at least 10 times higher than in either of the controls. Altogether 94 cellular proteins met these criteria.

The list of host proteins identified in VRCs was sorted based on both their cellular localization and molecular function (see Table 2). According to the functional

annotation program DAVID (Huang *et al.*, 2008; Huang *et al.*, 2009), less than 1% of the host proteins were ER- and approximately 14% chloroplast-associated in our proteome data. DAVID often places the same protein into several categories, e.g. based on both its cellular location and molecular function, which hampers the calculations. When all the proteins, whether having a localization or molecular function associated with chloroplasts, were combined manually, the amount of these proteins among all of the identified proteins raised to 25%. Among the most abundant ER proteins in the sample were Luminal binding protein 5 (BiP5) and calreticulin (Table S1). However, calreticulin, which is an HCpro binding partner (Shen *et al.*, 2010), did not meet all the criteria to enter the final list presented in Table 2. Of the chloroplast-associated proteins e.g. chloroplastic glyceraldehyde-3-phosphate dehydrogenase (GAPDH), carbonic anhydrase, a peripheral protein of the translocon at the chloroplast inner envelope, TIC110, and the outer envelope translocation channel,TOC75-3, were identified with high confidence (Table 2). While the relevance of some identified proteins, like for HSP70, HSP90, HSP40, eEF1A and GAPDH, is already known in (+)RNA virus multiplication (Castorena *et al.*, 2007; Davis *et al.*, 2007; Huang and Nagy, 2011; Li *et al.*, 2010; Okamoto *et al.*, 2006; Pogany *et al.*, 2008; Tomita *et al.*, 2003; Wang *et al.*, 2009; Wang and Nagy, 2008; Weeks *et al.*, 2010; Yi *et al.*, 2011), for most of the proteins the exact molecular function needs to be worked out in order to understand potyviral replication.

It has been suggested that potyviral VRCs contain ribosomes translating PVA RNA (Grangeon *et al.* 2010). To compare the content of ribosomal proteins, we looked at each proteome individually with more relaxed parameters. Ribosomal proteins for which peptides were found in at least two biological replicates amounting to at least three peptides, one of them unique, were selected. LC-MS/MS data shows that 16 out of the 32 small and 38 out of the 47 large ribosomal subunit proteins fulfilled

these criteria in the PVA-SC6K samples (Table 3). Importantly, the MC-SC6K control membranes pulled down none of the small and only 1 out of the 47 large ribosomal subunit proteins (L7a-1). PVA-C6K control also contained ribosomes as many ribosomal proteins were identified (17/47, 3/32) but most of them were less abundantly present than in the PVA-SC6K samples. This data suggests that a small portion of VRCs were binding also unspecifically to the Strep-Tactin matrix. These data indicate that the ribosomal proteins were very specifically associated with membranes active in virus replication.

Discussion

The focus of this work was to reveal the protein composition of the potyviral VRCs. To enable determination of the full viral and host protein content of the 6K2-induced membranous vesicles, we developed a purification strategy based on an affinity tag fused to 6K2 and exposed on the VRCs during PVA infection. Interesting questions relate to the orientation of 6K2 in the ER membranes. According to Lerich *et al.,* (2011) TEV 6K2 consists of an N-terminal cytoplasmic domain of 23 amino acids, a transmembrane (TM) domain of 19 amino acids, and a C-terminal putatively luminal domain of 11 amino acids. Our data from the SC6K carrying the N-terminal 2xStrep-CFP fusion supports this orientation (see Fig.3). Achieving this orientation would require the insertion of the SC6K with its C-terminus first into the ER lipid bilayer. The TM domain of potyviral 6K2 protein is located near the C-terminus, which is typical for the tail-anchored (TA) ER membrane proteins (reviewed in Johnson *et al.,* 2013). These proteins have a single C-terminal TM domain required to target them to and anchor in ER membrane. TA proteins form a topological group of membrane proteins, and like potyviral 6K2 protein, many of them are involved in vesicular transport (Ungar and Hughson, 2003). The N-terminus of TEV 6K2 contains a D(X)E

motif which is essential for ER exit of the 6K2-induced vesicles (Aniento *et al.*, 2006; Hanton *et al.*, 2005; Lerich *et al.*, 2011). However, the orientation question becomes more complicated when 6K2 is expressed from its natural context in the polyprotein. It is likely that the 6K2-VPg-Pro precursor serves as a scaffolding protein in leading to formation of the vesicle structures capable of supporting viral replication (Beauchemin *et al.,* 2007; Schaad *et al.,* 1997; Thivierge *et al.,* 2008). In this context the 6K2 TM domain would not anymore be C-terminal. Therefore, the question of 6K2-VPg-Pro orientation, which is likely a key factor determining the site of replication either inside the vesicles or on their surface, remains open for further studies.

In our analysis we aimed to identify proteins from vesicles that contain PVA replication complexes. Despite many tries, we could not demonstrate RNA synthesis activity within the purified PVA-SC6K vesicles. Nevertheless, approximately a 9-fold enrichment of PVA (+)-strand RNA was observed in PVA-SC6K compared to the PVA-C6K eluates. This demonstrates that major part of PVA RNA detected in PVA-SC6K was there because of tag-specific purification. As demonstrated by EM analysis of the eluates (see Fig. 5) some PVA particles were purified due to unspecific binding of particles to Strep-Tactin matrix, which likely explains the presence of PVA RNA in PVA-C6K eluate. The statistically significant difference in the fold of PVA RNA enrichment together with the presence of PVA (-)strand RNA in PVA-SC6K eluates suggests that PVA-SC6K sample likely contains membranes active in replication.

All PVA proteins except the PIPO-part of P3N-PIPO were detected in PVA-SC6K eluates. Therefore the two peptides from the P3N-region, which are common both for the P3 and P3N-PIPO, are with high probability derived from P3 protein. Due to very low amount of P1 peptides in LC-MS/MS data we do not consider P1 to be

specifically present. Because PVA particles were co-purified, CP was present partially un-specifically. CP was, however, enriched 3.6 fold compared to PVA-C6K control and therefore it is a borderline case whether it should be regarded to be present in VRCs. P1, CP and P3N-PIPO are the three proteins that are not needed for potyviral replication (Mahajan *et al.*, 1996; Verchot and Carrington, 1995; Wen and Hajimorad, 2010), which is supported by our findings. Peptides derived from HCpro and CI were abundantly found in the PVA-SC6K eluates and they were enriched 68- and 45-fold in comparison to PVA-C6K control, respectively. The presence of CI and HCpro in the PVA-C6K control may partially even result from the virions being un-specifically co-purified, as both CI and HCpro have been located at one of the extremities of PVA particles (Gabrenaite-Verkhovskaya *et al.*, 2008; Torrance *et al.*, 2006). The presence of NIb, VPg and NIa-Pro is a prerequisite to state that VRCs have been purified. All these were found unquestionably from the PVA-SC6K eluates. As the P3 of TEV has previously been shown to form punctate inclusions that co-localized with the 6K2 vesicles (Cui *et al.*, 2010), the specific detection of P3 supports our hypothesis. Taken together HCpro, P3, 6K1, CI, 6K2, VPg-NIpro and NIb are present in the purified 6K2-induced vesicles during PVA infection. However, further studies are required to investigate their relative abundances within the VRC.

It is proposed in the model for potyviral TuMV replication vesicle biogenesis presented by Grangeon *et al.* (2010) that viral translation and replication are tightly coupled within the virus-induced vesicles. This suggestion is based on the finding that vesicles derived from a single viral genome contained the proteins synthesized from that same viral RNA (Cotton *et al.*, 2009). This model states that ribosomes associated with viral factors and RNA on the ER membranes become trapped within the replication vesicles where viral protein synthesis then continues. Our LC-MS/MS

data revealed the presence of 38 60S and 16 40S ribosomal proteins in the PVA-SC6K eluates. Applying the same conditions to the MC-SC6K control proteome list there was only one ribosomal protein present, namely 60S ribosomal protein L7a-1. Therefore it can be suggested that ribosomes associate with VRCs in infected cells but not with 6K2-induced vesicles in the absence of infection. However, whether the ribosomes are internalized or exist on the outer surface of VRCs cannot be concluded from our data. Nevertheless, tight association between replication and translation, as suggested in Cotton *et al.* (2009) and Hafrén *et al.* (2010), is supported in the light of these data. Some of the ribosomal proteins found from the proteome data may also have more specific functions in potyviral multiplication. Yang *et al.* (2009) showed that replication of TuMV is inhibited in plants where RPL19, RPL13, RPL7, and RPS2 and RPS6 are silenced. Also acidic ribosomal protein P0 was present in the VRC proteome. In our earlier work we have identified P0 from PVA RNP complex associated with replication membranes and shown it to be essential for PVA RNA and virion accumulation in infection (Hafrén *et al.*, 2013).

Despite the fact that the PVA-SC6K induced vesicles were not found to associate with chloroplasts in the same way as the PVA-6KY vesicles when imaged by confocal microscopy, 25% of the host proteins in the final proteome were categorized as chloroplast-associated proteins. In the light of the proteome data it is therefore conceivable that PVA replication within the SC6K-containing vesicles occurs in association with chloroplasts and there is no contradiction with the previous literature stating that disrupting VRC-chloroplast fusion is detrimental for potyviral replication (Wei *et al.*, 2013). Several host factors that are linked with potyviral replication and localize to potyviral VRCs (reviewed in Revers and García, 2015) were identified. From these host factors HSP70 was the host protein most abundantly found in the samples. Moreover, eEF1A and initiation factor 4A (IF4A)

were both found from the VRC proteome confirming the previous findings. Many other cellular proteins with a confirmed role in (+)RNA virus replication were identified. GAPDH, which is essential for determination of (+) / (-)RNA synthesis ratio during tombusvirus infection (Huang and Nagy, 2011), is an example of such a protein. In summary, we conclude PVA-SC6K sample consists mostly of purified VRCs and the host proteins associated may have relevance in PVA replication. The next essential step will be to screen for those host proteins which have a role in PVA multiplication and to further analyze the detailed molecular function of each host protein.

Experimental procedures:

Plants, growth conditions, agroinfiltration

Nicotiana benthamiana was kept under greenhouse conditions with 22 °C day time and 18 °C night time temperatures. Plants were infiltrated with *Agrobacterium tumefaciens* in infiltration buffer (10 mM MES, 10 mM $MgCl_2$, 150 μM acetosyringone) at four to six leaf stage as described in Eskelin *et al*., (2010). Systemically infected plant leaves were harvested at 10 days after agroinfiltration (DPI), locally expressed constructs were harvested 4 days after agroinfiltration.

Constructs

Viral- and protein expression constructs used in this study were based on the full-length infectious cDNA copies of PVA strain B11 (GenBank accession number AJ296311).

PVA-C6K

CFP-6K2 fusion sequence was amplified from pSITEII-2C1 vector using primers XbaKpnCer, which adds XbaI and KpnI restriction sites in front of the cerulean sequence, and 6KR_Mlu, which adds MluI restriction site at the 3'-end of 6K2 sequence (Table S2). The PCR product was cloned to pGEM-T Easy vector producing pGEM-T Easy::Cerulean-6K2 vector.

SacII and MluI sites were used to transfer CFP-6K2 from pGEM-T Easy to pUC18::PVA^{WT} between NIb and CP sequence resulting in pUC18::PVA- Cerulean-6K2 (pUC18::PVA-C6) vector. PVA-Cerulean-6K2 was cloned to pRD400::PVA^{WT} agro vector using SalI and AgeI restriction sites resulting in pRD400::PVA-CFP-6K2 (PVA-C6K) vector.

PVA-SC6K

Twin Strep-tag II (2xStrep) sequence was amplified with PCR from pGEM-T Easy::2xStrep using SP6 and T7 primers. The PCR fragment was cut with XbaI and KpnI and inserted to same sites in pGEM-T Easy::CFP-6K2 resulting in pGEM-T Easy::2xStrep-CFP-6K2 vector.

SacII and MluI sites were used to transfer 2xStrep-CFP-6K2 from pGEM-T Easy to pUC18::PVA^{WT} between NIb and CP sequence resulting in pUC18::PVA-2xStrep-CFP-6K2 (pUC18::PVA-SC6) vector. PVA-2xStrep-CFP-6K2 was cloned to pRD400::PVA^{WT} agro vector using SalI and AgeI restriction sites resulting in pRD400::PVA-2xStrep-CFP-6K2 (PVA-SC6K) vector.

PVA-6KY

The potyviral 6K2 protein was PCR amplified from the PVA genome and inserted into pGWB41. The 6K2-YFP fusion was then amplified from the pGWB41-6K2 plasmid with primers AfI_6K and YFP_R (Table S2), which introduced AflII and MluI restriction sites in front and at the end of 6K2-YFP. These restriction sites were used

to clone the PCR fragment to the icDNA of PVA in pUC18 vector. From there the complete PVA icDNA with *CaMV 35S* promoter and *nos* terminator was cloned to pRD400 binary vector using KpnI and SalI restriction sites yielding PVA-6KY construct.

NIa protease cleavage sites flanked all insertions in between NIb and CP genes.

MC-SC6K

The control construct 2xStrep-CFP-6K2 was constructed as follows: 2xStrep-CFP-6K2 sequence was amplified from pGEM-T Easy::2xStrep-CFP-6K2 vector using primers 2xStrep_ATG_Xho_Fw and 6K2_stop_Bam_Rev (Table S2), resulting in a fragment that had XhoI restriction site and ATG translation initiation codon in front of 2xStrep sequence and a double TAA translation termination codon and BamHI restriction site at the 3' end of 6K2. This fragment was cloned to pANU vector that contained 35S promoter and *nos* transcription terminator, using XhoI and BamHI sites. The resulting 35S-2xStrep-CFP-6K2-term cassette was inserted to pRD400 agro-vector using HindIII site.

The correctness of all constructs was confirmed by sequencing.

Sample preparation

For LC-MS/MS analysis the vesicles were prepared as follows: 10 g of *Nicotiana benthamiana* leaves were homogenized in sampling buffer (13% sucrose, 50 mM Tris-HCl, 10 mM KCl, 3 mM $MgCl_2$, 1 mM EDTA, 1 mM DTT, 0.3% dextran, 0.1% BSA, pH 8) in the ratio of 1 g of leaves to 3 ml of buffer yielding 30 ml of sample. Initial centrifugation of homogenized material was carried out at 3000 g for 10 min at 4°C. Resulting supernatant, 13 ml per centrifugation tube, was loaded on top of discontinuous sucrose gradient (from the bottom: 8 ml 45%; 9 ml 30%; 9 ml 20%). Ultra centrifugation of samples on sucrose gradient was carried out in Beckman-

Coulter SW-28 rotor at 25 000 rpm (r_{av} approximately 83 000 x g) for 5 hours at 4°C. Fraction enriched in CFP signal (fraction 5), was used in the affinity purification step. Fraction 5 from two ultra-centrifugation tubes, 5 ml each, was combined. All samples were done in three biological replicates.

Affinity purification

Avidin (100 µg/ml) was added to the fraction of interest from ultracentrifugation and the sample was incubated on ice for 10 min. Affinity chromatography was carried out at room temperature by letting the sample flow through 0.5 ml (initially 1 ml of 50% slurry) of *Strep*-Tactin® Sepharose (IBA) resin by gravity flow. The column was washed with 5 ml (10x column bed volume) of ice-cold washing buffer (50 mM Tris-HCl, 10 mM KCl, 3 mM $MgCl_2$, pH 8). Samples were eluted with 2 ml of ice-cold washing buffer containing 1 mM biotin (Thermo Scientific). Samples were concentrated using Amicon® Ultra-4 Centrifugal Filter Units (Merck Millipore) with 10 kDa cut-off limit.

Electron microscopy

Thin sections were prepared as follows: infected leaf sample was taken under 0.1 M phosphate buffer ($NaPO_4$ pH 7.4). Leaf discs were de-gassed in 0.1 M phosphate buffer containing 2.5% glutaraldehyde and left for fixation at room temperature for 2 hours. After washing with 0.1 M phosphate buffer the samples were osmicated in the same buffer containing 1% OsO_4 for 1 hour at room temperature. The samples were then dehydrated with ethanol and acetone and embedded in Epon 812 (Taab Laboratories, Reading, UK). 90 nm sections were post-stained with 2% uranyl acetate and Reynold's lead-citrate. For negative staining of purified vesicles the sample was prepared as for LC-MS/MS, with the exception that elution was carried out with washing buffer containing 2.5 mM desthiobiotin. Purified vesicle samples

were viewed on Jeol 1400 transmission electron microscope. 1% phosphotungstic acid was used as the negative staining agent for purified 6K2-membrane samples.

Confocal microscopy

Confocal laser scanning microscopy was performed on a Leica TCS SP5II confocal microscope. Systemically infected *N. benthamiana* leaves were selected for confocal microscopy analysis 10 DPI for PVA icDNA constructs or locally infiltrated *N. benthamiana* leaves 4 DPI for the MC-SC6K construct. Small discs were cut from the *N. benhtamiana* leaves, mounted between cover and objective glass, immersed in water, and viewed with 20X objective. YFP excitation was carried out using argon laser at 514 nm while emission was recorded at 525-555 nm (DD 458/514 beam splitter). CFP excitation was carried out using argon laser at 458 nm while emission was recorded at 470-500 nm. Images represent 5 µm Z-stacks taken at 1 µm intervals. All images were deconvoluted using Autoquant X3 software and the presented images were obtained using Imaris software.

RT-PCR

Total RNA was extracted from 200 ul of sample using Trizol (Thermo Fisher Scientific) and taken up in 20 ul of nuclease free water. The purified RNA was DNase treated for 10 min at room temperature using 1 µl of DNaseI (1U/µl) and RDD buffer (Qiagen). cDNA was synthesized from 4 µl of RNA using Superscript III reverse transcriptase (Life technologies). Primer RT_CPminus_F was used to detect PVA genomic RNA of negative polarity and primer RT_CPplus_R to detect PVA genomic RNA of positive polarity (Table S2). Phusion polymerase (Finnzymes) with the same RT primers was used to amplify the coding region of PVA CP gene.

Quantitative real-time PCR

RNA was extracted using Trizol (Thermo Fischer Scientific) from 100 µl of input and affinity purified sample in three biological replicates for each construct and taken up in 20 µl of nuclease free water. The purified RNA was DNase treated for 10 min at room temperature using 1 µl of DNaseI (1U/µl) and RDD buffer (Qiagen). cDNA was synthesized from 5 µl of purified RNA using RevertAid H Minus First Strand cDNA Synthesis Kit (Thermo Scientific) and random hexamers. Quantitative real-time PCR was performed using Maxima SYBR Green qPCR kit (Thermo Scientific) and primers specific to PVA CP sequence, namely qPCR_CP_F and qPCR_CP_R (Table S2).

Protein identification by LC-MS/MS and Proteome analysis

Disulfide bridges in proteins were reduced with 50mM TCEP (Tris(2-carboxyethol)phosphine hydrochloride salt, Sigma-Aldrich) for 20 min at 37°C. To block cysteine residues, iodoacetamide (Fluka, Sigma-Aldrich) was added to a final concentration of 150 mM and the samples were incubated at room temperature in the dark for 30 min. A total of 0.75 µg trypsin (Promega) was added, and the samples were incubated overnight at 37 °C. Tryptic digests were quenched with 10% (v/v) trifluoroacetic acid (TFA) and purified using C18 microspin columns (Harvard Apparatus). Columns were eluted with 0.1% (v/v) TFA in 50% (v/v) acetonitrile (ACN) and the volume of the eluted samples was reduced to approximately 2 µl in a vacuum centrifuge. The peptides were reconstituted to a final volume of 30 µl with 0.1% (v/v) TFA, 1% (v/v) ACN and vortexed thoroughly. LC-MS/MS analysis was carried out using an EASY-nLC nano-HPLC system (Thermo Fisher Scientific) connected to a Velos Pro-Orbitrap Elite hybrid mass spectrometer (Thermo Fisher Scientific) with a nano-electrospray ion source (Thermo Fisher Scientific). A two-column setup was used, consisting of a 2 cm C18-A1 trap column (Thermo Fisher Scientific), followed by a 10 cm C18-A2 analytical column (Thermo Fisher Scientific).

Linear separation gradient was 5% (v/v) buffer B (0.1% TFA acid in 98% ACN) in 5 min, 35% (v/v) buffer B in 60 min, 80% (v/v) buffer B in 5 min and 100% buffer B in 10 min at a flow rate of 0.3 µl/min. 5 µl of sample was injected for SC6K and C6K and 3 µl for MC-SC6K LC-MS/MS runs. Full MS scan was acquired with a resolution of 60,000 over a normal mass range of the Orbitrap analyzer; the method was set to fragment the 20 most intense precursor ions with CID (energy 35). Data was acquired using LTQ Tune software. Acquired MS2 scans were searched against the *N. benthamiana* annotated protein database derived from solgenomics.net using the Sequest search algorithms in the Proteome Discoverer software (Thermo Fisher Scientific). Allowed mass error was 15 ppm for precursor ions and 0.8 Da for fragment ions. Carbamidomethylation (+57.021 Da) of cysteine was set as a static modification and oxidation of methionine (+15.995 Da) as a dynamic modification. Database searches were limited to fully tryptic peptides with maximum one missed cleavage. Web based bioinformatics database DAVID (Huang *et al.*, 2008; Huang *et al.*, 2009) was used as a guide for the classification of the proteins. For ribosomal protein lists the TAIR IDs of discovered proteins were submitted to DAVID functional annotation tool and the proteins classified as “ribosomal protein” were selected for the ribosomal protein lists.

Acknowledgements:

We thank Anders Hafrén for valuable discussions throughout this study, Minna Pöllänen for taking care of the plants and Sini Miettinen for assistance with the LC-MS/MS analysis. Dr Eija Jokitalo and Ms. Mervi Lindman at the EM unit of the Institute of Biotechnology, University of Helsinki are acknowledged for their help in EM imaging. Financial support given by the Academy of Finland (grants 1138329 to K.M. and 1258978 to M.V.) and Jenny and Antti Wihuri Foundation is gratefully acknowledged. A.L. was supported by the Integrative Life Science Doctoral Program

and Research Foundation of University of Helsinki. We declare that we have no conflict of interest.

References:

Aniento, F., Matsuoka, K. and Robinson, D.G. (2006) ER-to-Golgi Transport: The COPII-Pathway. In The Plant Endoplasmic Reticulum. (Robinson, D.G., ed), Plant Cell Monographs. pp. 99–124. Springer Berlin Heidelberg.

Anindya, R., Chittori, S. and Savithri, H.S. (2005) Tyrosine 66 of Pepper vein banding virus genome-linked protein is uridylylated by RNA-dependent RNA polymerase. *Virology* **336**, 154–162.

Barajas, D., Martín, I.F. de C., Pogany, J., Risco, C. and Nagy, P.D. (2014) Noncanonical Role for the Host Vps4 AAA+ ATPase ESCRT Protein in the Formation of Tomato Bushy Stunt Virus Replicase. *PLoS Pathog* **10**, e1004087.

Beauchemin, C., Boutet, N. and Laliberté, J.-F. (2007a) Visualization of the Interaction between the Precursors of VPg, the Viral Protein Linked to the Genome of Turnip Mosaic Virus, and the Translation Eukaryotic Initiation Factor iso 4E In Planta. *J. Virol.* **81**, 775–782.

Beauchemin, C., Boutet, N. and Laliberté, J.-F. (2007b) Visualization of the interaction between the precursors of VPg, the viral protein linked to the genome of turnip mosaic virus, and the translation eukaryotic initiation factor iso 4E in Planta. *J. Virol.* **81**, 775–782.

Boon, J.A. den and Ahlquist, P. (2010) Organelle-Like Membrane Compartmentalization of Positive-Strand RNA Virus Replication Factories. *Annu. Rev. Microbiol.* **64**, 241–256.

Carrington, J.C., Jensen, P.E. and Schaad, M.C. (1998) Genetic evidence for an essential role for potyvirus CI protein in cell-to-cell movement. *Plant J.* **14**, 393–400.

Castorena, K.M., Weeks, S.A., Stapleford, K.A., Cadwallader, A.M. and Miller, D.J. (2007) A Functional Heat Shock Protein 90 Chaperone Is Essential for Efficient Flock House Virus RNA Polymerase Synthesis in Drosophila Cells. *J. Virol.* **81**, 8412–8420.

Cotton, S., Grangeon, R., Thivierge, K., Mathieu, I., Ide, C., Wei, T., Wang, A. and Laliberté, J.-F. (2009) Turnip Mosaic Virus RNA Replication Complex Vesicles Are Mobile, Align with Microfilaments, and Are Each Derived from a Single Viral Genome. *J. Virol.* **83**, 10460–10471.

Cui, X., Wei, T., Chowda-Reddy, R.V., Sun, G. and Wang, A. (2010) The Tobacco etch virus P3 protein forms mobile inclusions via the early secretory pathway and traffics along actin microfilaments. *Virology* **397**, 56–63.

Davis, W.G., Blackwell, J.L., Shi, P.-Y. and Brinton, M.A. (2007) Interaction between the Cellular Protein eEF1A and the 3'-Terminal Stem-Loop of West Nile Virus Genomic RNA Facilitates Viral Minus-Strand RNA Synthesis. *J. Virol.* **81**, 10172–10187.

Dufresne, P.J., Thivierge, K., Cotton, S., Beauchemin, C., Ide, C., Ubalijoro, E., Laliberté, J.-F. and Fortin, M.G. (2008) Heat shock 70 protein interaction with Turnip mosaic virus RNA-dependent RNA polymerase within virus-induced membrane vesicles. *Virology* **374**, 217–227.

Eskelin, K., Suntio, T., Hyvärinen, S., Hafren, A. and Mäkinen, K. (2010) Renilla luciferase-based quantitation of Potato virus A infection initiated with Agrobacterium infiltration of N. benthamiana leaves. *J. Virol. Methods* **164**, 101–110.

Fernández, A., Guo, H.S., Sáenz, P., Simón-Buela, L., Gómez de Cedrón, M. and García, J.A. (1997) The motif V of plum pox potyvirus CI RNA helicase is involved in NTP hydrolysis and is essential for virus RNA replication. *Nucleic Acids Res.* **25**, 4474–4480.

Gabrenaite-Verkhovskaya, R., Andreev, I.A., Kalinina, N.O., Torrance, L., Taliansky, M.E. and Mäkinen, K. (2008) Cylindrical inclusion protein of potato virus A is associated with a subpopulation of particles isolated from infected plants. *J. Gen. Virol.* **89**, 829–838.

Grangeon, R., Agbeci, M., Chen, J., Grondin, G., Zheng, H. and Laliberté, J.-F. (2012) Impact on the endoplasmic reticulum and Golgi apparatus of turnip mosaic virus infection. *J. Virol.* **86**, 9255–9265.

Grangeon, R., Cotton, S. and Laliberté, J.-F. (2010) A model for the biogenesis of turnip mosaic virus replication factories. *Commun. Integr. Biol.* **3**, 363–365.

Hafrén, A., Eskelin, K. and Mäkinen, K. (2013) Ribosomal Protein P0 Promotes Potato Virus A Infection and Functions in Viral Translation Together with VPg and eIF(iso)4E. *J. Virol.* **87**, 4302–4312.

Hafrén, A., Hofius, D., Rönnholm, G., Sonnewald, U. and Mäkinen, K. (2010) HSP70 and Its Cochaperone CPIP Promote Potyvirus Infection in Nicotiana benthamiana by Regulating Viral Coat Protein Functions. *Plant Cell Online* **22**, 523–535.

Hanton, S.L., Renna, L., Bortolotti, L.E., Chatre, L., Stefano, G. and Brandizzi, F. (2005) Diacidic Motifs Influence the Export of Transmembrane Proteins from the Endoplasmic Reticulum in Plant Cells. *Plant Cell* **17**, 3081–3093.

Hong, Y. and Hunt, A.G. (1996) RNA Polymerase Activity Catalyzed by a Potyvirus-Encoded RNA-Dependent RNA Polymerase. *Virology* **226**, 146–151.

Huang, D.W., Sherman, B.T. and Lempicki, R.A. (2009) Bioinformatics enrichment tools: paths toward the comprehensive functional analysis of large gene lists. *Nucleic Acids Res.* **37**, 1–13.

Huang, D.W., Sherman, B.T. and Lempicki, R.A. (2008) Systematic and integrative analysis of large gene lists using DAVID bioinformatics resources. *Nat. Protoc.* **4**, 44–57.

Huang, T.-S. and Nagy, P.D. (2011) Direct Inhibition of Tombusvirus Plus-Strand RNA Synthesis by a Dominant Negative Mutant of a Host Metabolic Enzyme, Glyceraldehyde-3-Phosphate Dehydrogenase, in Yeast and Plants▽. *J. Virol.* **85**, 9090–9102.

Huang, Y.W., Hu, C.C., Liou, M.R., Chang, B.Y., Tsai, C.H., Meng, M., Lin, N.S. and Hsu, Y.H. (2012) Hsp90 interacts specifically with viral RNA and differentially regulates replication initiation of Bamboo mosaic virus and associated satellite RNA. *PLoS Pathog.* **8**, e1002726.

Johnson, N., Powis, K. and High, S. (2013) Post-translational translocation into the endoplasmic reticulum. *Biochim. Biophys. Acta BBA - Mol. Cell Res.* **1833**, 2403–2409.

Kekarainen, T., Savilahti, H. and Valkonen, J.P.T. (2002) Functional Genomics on Potato Virus A: Virus Genome-Wide Map of Sites Essential for Virus Propagation. *Genome Res.* **12**, 584–594.

Klein, P.G., Klein, R.R., Rodriguez-Cerezo, E., Hunt, A.G. and Shaw, J.G. (1994) Mutational Analysis of the Tobacco Vein Mottling Virus Genome. *Virology* **204**, 759–769.

Lerich, A., Langhans, M., Sturm, S. and Robinson, D.G. (2011) Is the 6 kDa tobacco etch viral protein a bona fide ERES marker? *J. Exp. Bot.* **62**, 5013–5023.

Li, Z., Pogany, J., Tupman, S., Esposito, A.M., Kinzy, T.G. and Nagy, P.D. (2010) Translation Elongation Factor 1A Facilitates the Assembly of the Tombusvirus Replicase and Stimulates Minus-Strand Synthesis. *PLoS Pathog* **6**, e1001175.

Mahajan, S., Dolja, V.V. and Carrington, J.C. (1996) Roles of the sequence encoding tobacco etch virus capsid protein in genome amplification: requirements for the translation process and a cis-active element. *J. Virol.* **70**, 4370–4379.

Miller, S. and Krijnse-Locker, J. (2008) Modification of intracellular membrane structures for virus replication. *Nat. Rev. Microbiol.* **6**, 363–374.

Mine, A. and Okuno, T. (2012) Composition of plant virus RNA replicase complexes. *Curr. Opin. Virol.* **2**, 669–675.

Nagy, P.D. and Pogany, J. (2012) The dependence of viral RNA replication on co-opted host factors. *Nat. Rev. Microbiol.* **10**, 137–149.

Okamoto, T., Nishimura, Y., Ichimura, T., Suzuki, K., Miyamura, T., Suzuki, T., Moriishi, K. and Matsuura, Y. (2006) Hepatitis C virus RNA replication is regulated by FKBP8 and Hsp90. *EMBO J.* **25**, 5015–5025.

Olspert, A., Chung, B.Y.-W., Atkins, J.F., Carr, J.P. and Firth, A.E. (2015) Transcriptional slippage in the positive-sense RNA virus family Potyviridae. *EMBO Rep.* **16**, 995–1004.

Paul, D. and Bartenschlager, R. (2013) Architecture and biogenesis of plus-strand RNA virus replication factories. *World J. Virol.* **2**, 32–48.

Paul, D., Hoppe, S., Saher, G., Krijnse-Locker, J. and Bartenschlager, R. (2013) Morphological and Biochemical Characterization of the Membranous Hepatitis C Virus Replication Compartment. *J. Virol.* **87**, 10612–10627.

Pogany, J. and Nagy, P.D. (2008) Authentic Replication and Recombination of Tomato Bushy Stunt Virus RNA in a Cell-Free Extract from Yeast. *J. Virol.* **82**, 5967–5980.

Pogany, J., Stork, J., Li, Z. and Nagy, P.D. (2008) In vitro assembly of the Tomato bushy stunt virus replicase requires the host Heat shock protein 70. *Proc. Natl. Acad. Sci.*, pnas.0810851105.

Puustinen, P. and Mäkinen, K. (2004) Uridylylation of the Potyvirus VPg by Viral Replicase NIb Correlates with the Nucleotide Binding Capacity of VPg. *J. Biol. Chem.* **279**, 38103–38110.

Rajamäki, M.-L. and Valkonen, J.P.T. (1999) The 6K2 Protein and the VPg of Potato Virus A Are Determinants of Systemic Infection in Nicandra physaloides. *Mol. Plant. Microbe Interact.* **12**, 1074–1081.

Rantalainen, K.I., Eskelin, K., Tompa, P. and Mäkinen, K. (2011) Structural Flexibility Allows the Functional Diversity of Potyvirus Genome-Linked Protein VPg. *J. Virol.* **85**, 2449–2457.

Revers, F. and García, J.A. (2015) Chapter Three - Molecular Biology of Potyviruses. In Advances in Virus Research. (Mettenleiter, K.M. and T.C., ed), pp. 101–199. Academic Press.

Rodamilans, B., Valli, A., Mingot, A., San León, D., Baulcombe, D., López-Moya, J.J. and García, J.A. (2015) RNA polymerase slippage as a mechanism for the production of frameshift gene products in plant viruses of the potyviridae family. *J. Virol.* **89**, 6965–6967.

Schaad, M.C., Jensen, P.E. and Carrington, J.C. (1997) Formation of plant RNA virus replication complexes on membranes: role of an endoplasmic reticulum-targeted viral protein. *EMBO J.* **16**, 4049–4059.

Schmidt, T.G. and Skerra, A. (2007) The Strep-tag system for one-step purification and high-affinity detection or capturing of proteins. *Nat. Protoc.* **2**, 1528–1535.

Shen, W., Yan, P., Gao, L., Pan, X., Wu, J. and Zhou, P. (2010) Helper component-proteinase (HC-Pro) protein of Papaya ringspot virus interacts with papaya calreticulin. *Mol. Plant Pathol.* **11**, 335–346.

Spetz, C. and Valkonen, J.P.T. (2004) Potyviral 6K2 Protein Long-Distance Movement and Symptom-Induction Functions Are Independent and Host-Specific. *Mol. Plant. Microbe Interact.* **17**, 502–510.

Thivierge, K., Cotton, S., Dufresne, P.J., Mathieu, I., Beauchemin, C., Ide, C., Fortin, M.G. and Laliberté, J.-F. (2008) Eukaryotic elongation factor 1A interacts with Turnip mosaic virus RNA-dependent RNA polymerase and VPg-Pro in virus-induced vesicles. *Virology* **377**, 216–225.

Tomita, Y., Mizuno, T., Díez, J., Naito, S., Ahlquist, P. and Ishikawa, M. (2003) Mutation of Host dnaJ Homolog Inhibits Brome Mosaic Virus Negative-Strand RNA Synthesis. *J. Virol.* **77**, 2990–2997.

Torrance, L., Andreev, I.A., Gabrenaite-Verhovskaya, R., Cowan, G., Mäkinen, K. and Taliansky, M.E. (2006) An Unusual Structure at One End of Potato Potyvirus Particles. *J. Mol. Biol.* **357**, 1–8.

Ungar, D. and Hughson, F.M. (2003) SNARE protein structure and function. *Annu. Rev. Cell Dev. Biol.* **19**, 493–517.

Verchot, J. (2011) Wrapping membranes around plant virus infection. *Curr. Opin. Virol.* **1**, 388–395.

Verchot, J. and Carrington, J.C. (1995) Evidence that the potyvirus P1 proteinase functions in trans as an accessory factor for genome amplification. *J. Virol.* **69**, 3668–3674.

Wang, A. (2015) Dissecting the Molecular Network of Virus-Plant Interactions: The Complex Roles of Host Factors. *Annu. Rev. Phytopathol.* **53**, 45–66.

Wang, R.Y.-L. and Nagy, P.D. (2008) Tomato bushy stunt virus Co-Opts the RNA-Binding Function of a Host Metabolic Enzyme for Viral Genomic RNA Synthesis. *Cell Host Microbe* **3**, 178–187.

Wang, R.Y.-L., Stork, J. and Nagy, P.D. (2009) A Key Role for Heat Shock Protein 70 in the Localization and Insertion of Tombusvirus Replication Proteins to Intracellular Membranes. *J. Virol.* **83**, 3276–3287.

Weeks, S.A., Shield, W.P., Sahi, C., Craig, E.A., Rospert, S. and Miller, D.J. (2010) A Targeted Analysis of Cellular Chaperones Reveals Contrasting Roles for Heat Shock Protein 70 in Flock House Virus RNA Replication. *J. Virol.* **84**, 330–339.

Wei, T., Huang, T.-S., McNeil, J., Laliberté, J.-F., Hong, J., Nelson, R.S. and Wang, A. (2010) Sequential Recruitment of the Endoplasmic Reticulum and Chloroplasts for Plant Potyvirus Replication. *J. Virol.* **84**, 799–809.

Wei, T. and Wang, A. (2008) Biogenesis of Cytoplasmic Membranous Vesicles for Plant Potyvirus Replication Occurs at Endoplasmic Reticulum Exit Sites in a COPI- and COPII-Dependent Manner. *J. Virol.* **82**, 12252–12264.

Wei, T., Zhang, C., Hou, X., Sanfaçon, H. and Wang, A. (2013) The SNARE Protein Syp71 Is Essential for Turnip Mosaic Virus Infection by Mediating Fusion of Virus-Induced Vesicles with Chloroplasts. *PLoS Pathog.* **9**.

Wen, R.-H. and Hajimorad, M.R. (2010) Mutational analysis of the putative pipo of soybean mosaic virus suggests disruption of PIPO protein impedes movement. *Virology* **400**, 1–7.

Yang, C., Zhang, C., Dittman, J.D. and Whitham, S.A. (2009) Differential requirement of ribosomal protein S6 by plant RNA viruses with different translation initiation strategies. *Virology* **390**, 163–173.

Yi, Z., Sperzel, L., Nürnberger, C., et al. (2011) Identification and Characterization of the Host Protein DNAJC14 as a Broadly Active Flavivirus Replication Modulator. *PLoS Pathog* **7**, e1001255.

Supporting information

Table S1. Lists all of the unique proteins with Sum PSM and Peptides and Unique peptides.

Table S2. List of primers used in this study.

Fig. S1. Western blot of PVA CP in PVA-C6K and PVA-6KY infected plants.

Fig. S2. Protein concentrations in the affinity purified samples.

Fig. S3. PVA RNA amount in the affinity purification input and pull-down of PVA-SC6K and PVA-C6K samples.

Table 1. Viral proteins identified by mass spectrometry analysis from PVA-SC6K purification samples.

Viral protein	Σ# Coverage	Σ# Unique Peptides	Σ# Peptides	Σ# PSMs	PVA-SC6K/ PVA-C6K[a]
SC6K2	79,49	27	40	613	n.f.
CI	54,02	27	27	137	68,5
HCpro	59,52	22	22	136	45,3
P3 (P3N-PIPO)[b]	41,79	12 (2)	12	66	n.f.
VPg	71,96	12	12	57	n.f.
Nib	43,99	14	14	48	n.f.
Nia	54,94	8	8	27	n.f.
CP	31,65	5	5	18	3,6
6K1	46,15	3	3	9	n.f.
P1	7,72	1	1	1	n.f.
PIPO[c]	0,00	0	0	0	n.f.

a. Enrichment of viral proteins in PVA-SC6K over PVA-C6K sample
b. Two peptides match to the N-terminal part of P3 that can account for both P3 and P3N-PIPO
c. No peptides from the +2 frame of PIPO were identified
n.f., not found in PVA-C6K sample

Table 2. Proteome of affinity purified PVA 6K2-induced vesicles, location- and function based classification.

Category	TAIR ID	*N. benthamiana* ID[a] (solgenomics.net)	Name[b]	Σ# Unique peptides	Σ# Peptides	Σ# PSM	Σ Coverage
Chaperone							
	AT5G02500	NbS00025223g0018.1	HSC70-1	6	18	95	42,47
	AT5G02500	NbS00016136g0003.1	HSC70-1	3	17	92	39,59
	AT3G12580	NbS00009983g0008.1	HSP70	2	15	89	51,82
	AT5G50920	NbS00017400g0004.1	ATP-dependent Clp protease ATP-binding subunit clpA homolog CD4B, chloroplastic	2	26	55	38,15
	AT5G28540	NbS00040865g0006.1	Luminal-binding protein 5	6	8	26	14,81
	AT5G56030	NbS00025260g0001.1	HSP81-2	3	10	22	23,7
	AT5G56030	NbS00021897g0010.1	HSP81-2	4	11	21	18,99
	AT4G24280	NbS00052944g0006.1	Chloroplast heat shock protein 70-1	10	10	18	17,47
	AT5G22060	NbS00016695g0014.1	DNAJ homologue 2	3	8	18	28,27
	AT3G48870	NbC25340200g0001.1	ATP-dependent Clp protease ATP-binding subunit clpA homolog CD4B, chloroplastic	2	7	17	64,43
	AT5G22060	NbS00004100g0004.1	DNAJ homologue 2	2	7	15	22,15
	AT3G13470	NbS00034791g0001.1	Chaperonin 60 subunit beta 2, chloroplastic	4	4	8	9,05
	AT4G24190	NbS00013845g0026.1	Heat shock protein 90	4	4	5	5,65
Chloroplast							
	AT2G39730	NbS00047700g0013.1	Ribulose bisphosphate carboxylase/oxygenase activase 2, chloroplastic	2	15	62	43,53
	AT1G06950	NbS00009678g0004.1	Protein TIC110, chloroplastic	9	23	59	32,34
	AT2G39730	NbS00009714g0011.1	Ribulose bisphosphate carboxylase/oxygenase activase 2, chloroplastic	2	14	56	47,8
	AT3G01500	NbS00016159g0006.1	Carbonic anhydrase, chloroplastic	3	10	53	43,71
	AT3G46740	NbS00002677g0011.1	Protein TOC75-3	14	14	50	30,02
	AT1G06950	NbS00021174g0005.1	Protein TIC110, chloroplastic	3	17	38	23,96
	AT4G02510	NbS00024250g0002.1	Translocase of chloroplast 159, chloroplastic	13	13	30	16,47
	AT3G47520	NbS00008675g0002.1	Malate dehydrogenase, chloroplastic	5	8	18	29,25
	AT5G38410	NbS00022486g0001.1	Ribulose bisphosphate carboxylase small chain 8B, chloroplastic	5	6	18	44,75
	AT2G20260	NbS00003075g0011.1	Photosystem I reaction center subunit IV B, chloroplastic	2	6	18	53,15

	AT2G24820	NbS00029739g0004.1	Translocon at the inner envelope membrane of chloroplasts 55-II	2	5	16	18,2
	AT3G56940	NbS00020307g0015.1	Magnesium-protoporphyrin IX monomethyl ester [oxidative] cyclase, chloroplastic protein, putative (Crd1)	7	7	15	19,55
	AT5G16620	NbS00017610g0108.1	Translocon at the inner envelope membrane of chloroplasts 40	3	5	15	15,41
	AT1G61520	NbS00021892g0003.1	Chlorophyll a-b binding protein 8	3	4	13	30,56
	AT1G74470	NbS00056940g0001.1	Geranylgeranyl diphosphate reductase, chloroplastic	5	5	12	14,22
	AT5G05000	NbS00005332g0008.1	Translocon at the outer envelope membrane of chloroplasts 34	4	4	12	25,58
	AT4G23430	NbS00010186g0028.1	Short-chain dehydrogenase TIC 32	4	4	11	25,08
	AT2G16640	NbS00010608g0012.1	Translocase of chloroplast 132, chloroplastic	3	7	10	5,77
	AT2G28000	NbS00033391g0006.1	RuBisCO large subunit-binding protein subunit alpha, chloroplastic	4	4	10	11,29
	AT2G16640	NbS00004829g0016.1	Translocase of chloroplast 132, chloroplastic	2	6	9	5,17
	AT2G38040	NbS00026142g0005.1	Acetyl-coenzyme A carboxylase carboxyl transferase subunit alpha, chloroplastic	4	5	8	12,61
	AT1G77590	NbS00027106g0001.1	LACS9, Long chain acyl-CoA synthetase 9, chloroplastic	4	4	8	9,95
	AT5G16620	NbS00033277g0017.1	Protein TIC 40, chloroplastic	2	4	8	20,29
	AT2G05100	NbS00019403g0016.1	Chlorophyll a-b binding protein 37, chloroplastic	3	4	7	22,26
Cytoplasm							
	AT1G62020	NbS00031319g0001.1	Coatomer subunit alpha-1	2	4	8	4,75
Cytoskeleton							
	AT1G75780	NbS00056603g0002.1	Tubulin beta-1 chain	2	12	49	39,39
	AT5G23860	NbS00001148g0004.1	Tubulin beta-8 chain	1	9	44	30,72
	AT4G14960	NbS00001594g0015.1	Tubulin alpha-6 chain	9	9	27	32,55
	AT5G12250	NbS00023211g0007.1	Tubulin beta-6 chain	2	8	19	30,15
Metabolic enzyme							
	AT1G12900	NbS00001169g0153.1	Glyceraldehyde 3-phosphate dehydrogenase A subunit 2	10	12	59	38,42
	AT4G35000	NbS00062043g0007.1	L-ascorbate peroxidase 3, peroxisomal	4	10	31	37,09
	AT3G27820	NbS00023324g0005.1	Probable monodehydroascorbate reductase, cytoplasmic isoform	10	10	30	23,81
	AT4G35000	NbS00035202g0004.1	L-ascorbate peroxidase 3, peroxisomal	2	7	26	37,77

	AT3G16950	NbS00014159g0003.1	Dihydrolipoyl dehydrogenase	4	8	21	19,07
	AT2G34590	NbS00007894g0004.1	Pyruvate dehydrogenase E1 component subunit beta	6	6	17	22,74
	AT1G01090	NbS00017334g0012.1	Pyruvate dehydrogenase E1 component subunit alpha	4	6	15	20,29
	AT1G01090	NbS00034265g0006.1	Pyruvate dehydrogenase E1 component subunit alpha	4	6	12	17,45
	AT2G22780	NbS00002298g0008.1	Malate dehydrogenase, glyoxysomal	5	5	11	16,87
	AT3G14420	NbS00005125g0015.1	Peroxisomal (S)-2-hydroxy-acid oxidase	6	6	8	24,44
	AT4G35090	NbS00006116g0019.1	Catalase isozyme 1	5	5	8	17,97
	AT1G44170	NbS00047628g0009.1	Aldehyde dehydrogenase	4	4	7	10,48
Nucleotide binding							
	AT4G17170	NbS00004361g0010.1	Ras-related protein RABB1c	6	6	19	37,44
	AT5G27540	NbS00036282g0010.1	MIRO-related GTP-ase 1	4	11	17	28,59
	AT2G27600	NbS00006021g0010.1	AAA-type ATPase family protein |	8	8	17	31,34
	AT1G78900	NbS00033958g0004.1	V-type proton ATPase catalytic subunit A	6	6	13	14,36
Ribosome/ protein biosynthesis							
	AT4G10450	NbS00002134g0112.1	Ribosomal protein L6 family	2	11	34	61,47
	AT2G27710	NbS00029619g0005.1	60S acidic ribosomal protein P2	3	5	13	42,95
	AT2G19730	NbS00054743g0008.1	Ribosomal L28e protein family	5	6	12	27,68
	AT4G09800	NbS00056355g0003.1	S18 ribosomal protein	2	4	12	32,24
	AT1G61580	NbS00018918g0016.1	R-protein L3 B	3	7	11	18,77
	AT3G13920	NbS00044851g0011.1	Eukaryotic translation initiation factor 4A1	5	5	10	15,98
	AT1G48830	NbS00039588g0004.1	Ribosomal protein S7e family protein	4	4	10	30,96
	AT1G61580	NbS00045996g0004.1	60S ribosomal protein L3	3	7	9	18,77
	AT3G49910	NbS00036380g0001.1	60S ribosomal protein L26-1	2	5	9	32,19
	AT1G57720	NbS00006811g0211.1	Probable elongation factor 1-gamma 2	4	4	9	9,38
	AT3G11250	NbS00018504g0008.1	60S acidic ribosomal protein P0	5	5	8	30,87
Other							
	AT1G04690	NbS00043430g0001.1	Probable voltage-gated potassium channel subunit beta; KAB1, KV-BETA1	13	13	71	64,75
	AT1G34430	NbC26077604g0003.1	Dihydrolipoyllysine-residue acetyltransferase component of pyruvate dehydrogenase complex	2	8	26	30,49
	AT5G08540	NbS00000164g0018.1	Unknown protein	9	9	21	34,58
	AT3G13930	NbS00000479g0101.1	Dihydrolipoyllysine-residue acetyltransferase component 2 of pyruvate dehydrogenase complex, mitochondrial	8	8	19	19,78

AT1G11910	NbS00028367g0004.1	Aspartic proteinase A1	2	6	19	17,98
AT5G24650	NbS00016191g0009.1	Mitochondrial import inner membrane translocase subunit Tim17/Tim22/Tim23 family protein	6	6	18	26,92
AT1G11910	NbS00031482g0006.1	Aspartic proteinase A1	2	6	17	17,39
AT3G01280	NbS00027615g0006.1	Voltage dependent anion channel 1	2	4	17	23,91
AT5G12470	NbS00005727g0008.1	Unknown	6	7	15	26,77
AT1G17860	NbC24872723g0001.1	Kunitz family trypsin and protease inhibitor protein	5	5	15	35,85
AT1G05270	NbS00011400g0014.1	TraB family protein	3	7	14	25,92
AT2G38040	NbS00048878g0013.1	CAC3, acetyl Co-enzyme a carboxylase carboxyltransferase alpha subunit	9	10	13	16,33
AT5G22640	NbS00044837g0004.1	emb1211, MORN (Membrane Occupation and Recognition Nexus) repeat-containing protein	7	7	13	14,47
AT1G33970	NbS00011570g0012.1	P-loop containing nucleoside triphosphate hydrolases superfamily protein	5	5	13	13,86
AT2G28900	NbS00045823g0014.1	Outer plastid envelope protein 16-1	4	4	13	26,75
AT5G62810	NbS00031622g0006.1	Peroxisomal membrane protein PEX14	2	5	11	36,63
AT1G10510	NbS00019582g0003.1	emb2004, RNI-like superfamily protein	6	6	10	19,64
AT2G20580	NbS00013228g0016.1	26S proteasome regulatory subunit S2 1A	2	5	8	9,7
AT1G11910	NbS00050653g0003.1	Aspartic proteinase A1	4	4	8	11,42
AT2G17840	NbS00004850g0017.1	ERD7, Senescence/dehydration-associated protein-related	5	5	7	16,82
AT3G57090	NbS00059906g0004.1	BIGYIN, FIS1A; Tetratricopeptide repeat (TPR)-like superfamily protein	4	4	7	27,97
AT5G62810	NbS00005874g0019.1	Peroxisomal membrane protein PEX14	3	4	7	18,94
AT2G44640	NbS00028734g0022.1	Uncharacterized protein	4	4	6	13,8
AT4G36720	NbS00015416g0013.1	HVA22-like protein K	4	4	5	30,48
AT2G32730	NbS00029577g0007.1	26S proteasome regulatory complex, non-ATPase subcomplex, Rpn2/Psmd1 subunit	4	4	5	8,39

[a] Derived from *N. benthamiana* annotated transcriptome list v0.4.4 (solgenomics.net)
[b] Derived from the *N. benthamiana* annotated transcriptome list v0.4.4 (solgenomics.net) or from closest WU-BLAST match in TAIR web-page

Table 3. Ribosomal proteins found in the PVA-SC6K sample.

TAIR ID	Name	Σ# PSM	Σ Coverage	PVA-SC6K/[a] PVA-C6	PVA-SC6K/[b] MC-SC6K
AT4G00100	40S ribosomal protein S13-2	11	26,32		
AT3G11510	40S ribosomal protein S14-2	12	38,67	2,40	
AT2G09990	40S ribosomal protein S16-1	4	17,01		
AT5G04800	40S ribosomal protein S17-4	7	16,67		
AT4G09800	40S ribosomal protein S18	10	26,32		
AT1G58684	40S ribosomal protein S2-2	5	15,36	1,25	
AT3G09680	40S ribosomal protein S23-1	4	20,18		
AT4G39200	40S ribosomal protein S25-4	10	33,02		
AT2G40590	40S ribosomal protein S26-1	4	25		
AT2G31610	40S ribosomal protein S3-1	8	23,21		
AT5G56670	40S ribosomal protein S30	3	16,13		
AT4G34670	40S ribosomal protein S3a-2	6	17,77	2,00	
AT3G11940	40S ribosomal protein S5-2	10	22,97		
AT4G31700	40S ribosomal protein S6-1	3	12,5		
AT1G48830	40S ribosomal protein S7-1	10	30,96		
AT5G59240	40S ribosomal protein S8-2	10	19,13		
AT3G11250	60S acidic ribosomal protein P0-3	8	30,87	2,67	
AT5G47700	60S acidic ribosomal protein P1-3	5	18,18		
AT2G27710	60S acidic ribosomal protein P2-2	7	30,09	1,40	
AT1G26910	60S ribosomal protein L10-2	9	17,81		
AT1G08360	60S ribosomal protein L10a-1	11	20,83	1,22	
AT5G45775	60S ribosomal protein L11-2	4	8,81		
AT2G37190	60S ribosomal protein L12-1	11	36,63	2,75	
AT3G49010	60S ribosomal protein L13-1	3	26,67	1,13	
AT3G07110	60S ribosomal protein L13a-1	3	15,48	0,75	
AT2G20450	60S ribosomal protein L14-1	4	15,69		
AT4G16720	60S ribosomal protein L15-1	8	19,61	2,67	
AT1G27400	60S ribosomal protein L17-1	3	14,6		
AT3G05590	60S ribosomal protein L18-2	6	21,61	1,13	
AT3G16780	60S ribosomal protein L19-2	5	19,07	1,67	
AT1G09690	60S ribosomal protein L21-1	6	32,32		
AT3G05560	60S ribosomal protein L22-2	6	32,26		
AT3G04400	60S ribosomal protein L23	11	46,43		
AT3G55280	60S ribosomal protein L23a-2	10	37,14	3,33	
AT2G36620	60S ribosomal protein L24-1	3	16,44	0,90	
AT3G49910	60S ribosomal protein L26-1	9	32,19		
AT4G15000	60S ribosomal protein L27-3	4	19,23		
AT2G19730	60S ribosomal protein L28-1	12	27,68		
AT1G61580	60S ribosomal protein L3-2	9	18,77		
AT4G18100	60S ribosomal protein L32-1	5	50,62		
AT1G26880	60S ribosomal protein L34-1	5	27,5	2,50	
AT1G74270	60S ribosomal protein L35a-3	4	28,57		
AT4G14320	60S ribosomal protein L36a	5	20,88		
AT3G09630	60S ribosomal protein L4-1	17	20,51	1,70	
AT1G74060	60S ribosomal protein L6-2	12	28,63		

AT1G74050	60S ribosomal protein L6-3	5	12,31		
AT2G01250	60S ribosomal protein L7-2	12	29,17		
AT3G13580	60S ribosomal protein L7-4	12	26,03		
AT2G47610	60S ribosomal protein L7a-1	7	22,09		1,75
AT3G62870	60S ribosomal protein L7a-2	7	22,09		
AT4G36130	60S ribosomal protein L8-3	13	28,85	2,60	
AT1G33140	60S ribosomal protein L9-1	28	55,15		
AT4G10450	60S ribosomal protein L9-2	34	61,47	11,33	
AT3G52590	NEDD8-like protein RUB1;60S ribosomal protein L40;40S ribosomal protein S27a-1;40S ribosomal protein S27a-3; Ubiquitin	3	14,93		
AT3G10950	Putative60S ribosomal protein L37a-1	5	27,17		

a. Enrichment of viral proteins in PVA-SC6K over PVA-C6K sample
b. Enrichment of viral proteins in PVA-SC6K over MC-SC6K sample

Figure legends:

Fig. 1. A schematic representation of the constructs. PVA-SC6K construct allows expression of 2xStrep-CFP-6K2 (SC6K2)-fusion protein in the context of PVA infection. PVA-C6K construct is similar, except it lacks the 2xstrep-tag. SC6K2-fusion is expressed from MC-SC6K construct (MC- membrane control) in a non-infected background. PVA-6KY construct allows expression of 6K2-Yellow fluorescent protein (6KY) fusion in PVA infection context. Dashed rectangles flanking the fluorescent protein - 6K2 cassettes denote NIa protease cleavage sites.

Fig. 2. PVA-C6K and PVA-6KY are both infectious and N-terminal 6K2 tag is accessible for affinity purification. a) Comparison of fluorescence derived from C6K (green) and 6KY (green) during PVA infection by confocal microscopy. C6K protein localized mostly to scattered vesicles whereas 6KY signal was detected mostly in association with chloroplasts (chl., red). Magnified sections show 6K2 vesicle-association with chloroplasts. b) Electron microscopy images of the infected tissues. Both PVA-C6K and PVA-6KY produced cytoplasmic cylindrical inclusions which are indicated with arrow heads. c) Affinity chromatography purification of the 6K2-fusion protein from the infection context reveals N-terminally fused CFP to be better accessible for the GFP-trap matrix compared to C-terminally fused YFP. d) A Western blot analysis verified the presence of PVA CP in the upper leaves 10 DPI indicating that PVA-SC6K, PVA-C6K and PVA-6KY are all able to cause systemic infection.

Fig. 3. Purification of 6K2-associated membranes from PVA infection. a) A schematic representation of the purification protocol. PVA-SC6K and PVA-C6K infected and SC6K expressing leaf tissues were homogenized and the cleared lysates were subjected to sucrose gradient centrifugation. Fraction 5 collected from the gradient was subjected to affinity purification via the 2x-strep-tag. b) The sucrose gradient fractions were analyzed by a Western blot analysis. SC6K concentrated to fraction 5 in the infection context and to fractions 5-7 when SC6K was expressed alone. c) Purified SC6K protein and its binding partners were subjected to 2xStrep-tag affinity purification. SC6K protein was significantly enriched in the eluate. The Twin-Strep-tag specific purification was controlled with tag-less C6K protein. (F.T. for flow through) d) The outcome of the purification procedure was assessed by SDS-PAGE followed by silver staining, which revealed clear differences in the protein

content between the purified PVA-SC6K sample in the left panel and the controls, PVA-C6K in the left panel and MC-SC6K in the right panel.

Fig. 4. PVA RNA and VPg content in the purified 6K2-associated membrane samples. a) Copy number of PVA RNA molecules (left panel) in the input and eluate of PVA-SC6K and PVA-C6K samples was determined by qRT-PCR. Mean values from three independent biological experiments, including three technical replicates each, are given. Error bars indicate standard deviations of mean. Note the logarithmic scale. Percentage of recovered RNA (right panel) indicates significant enrichment of PVA RNA in PVA-SC6K sample when compared to PVA-C6K sample. *, $P<0.05$. b) The presence of viral (+) and (-) RNA in the column eluates of PVA-SC6K, PVA-C6K and MC-SC6K samples was analysed by RT-PCR. RNA samples from 2xstrep-tag purifications were incubated prior to PCR with (+) or without (-) reverse transcriptase either in the presence of a (-)-strand or a (+)-strand specific primer. c) Replication protein VPg was detected by Western blotting with anti-VPg antibody in PVA-SC6K samples, but not in the control PVA-C6K.

Fig. 5. Morphological characterization of the purified 6K2-associated membranes. Affinity purified PVA-SC6K, PVA-C6K and MC-SC6K samples were negatively stained with uranyl-acetate and examined by TEM. Two types of membrane structures were observed: individual vesicles (left panels; shown by arrowheads) and membrane clusters (middle panels). Strep-tactin matrix captured PVA particles un-specifically from infected samples (right panels). The sizes of the purified individual vesicles vary between 50-100 nm while the median size is 56 nm (n = 40). Scale bar = 500 nm.

Construct name

Illustration

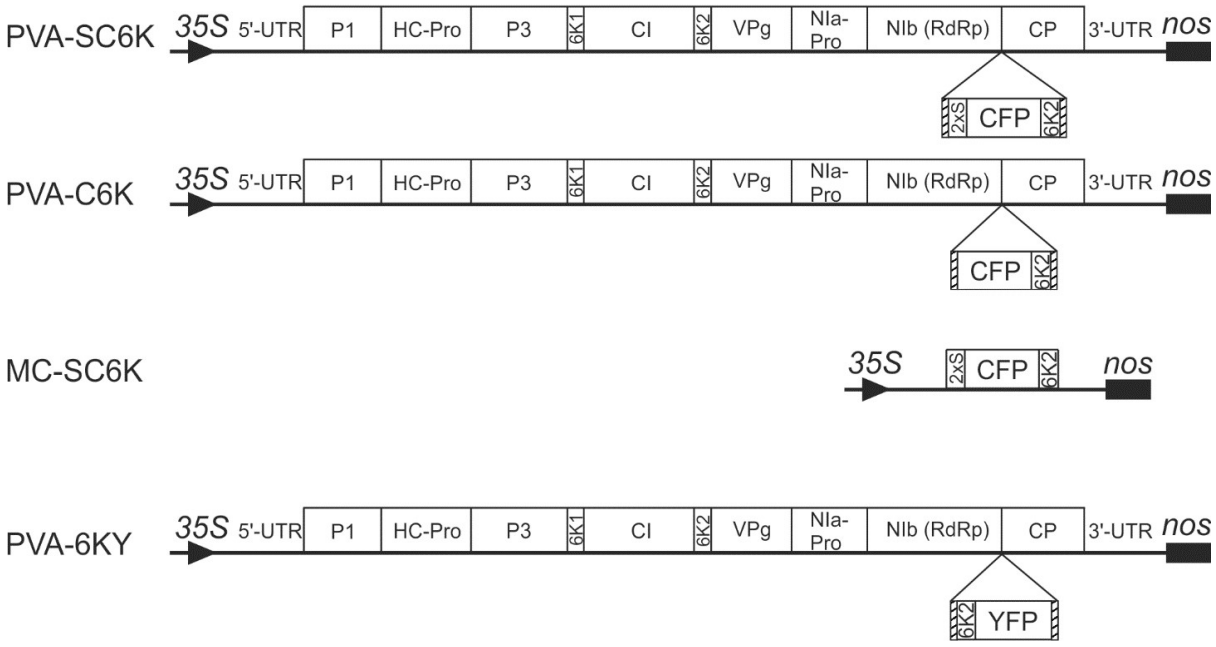

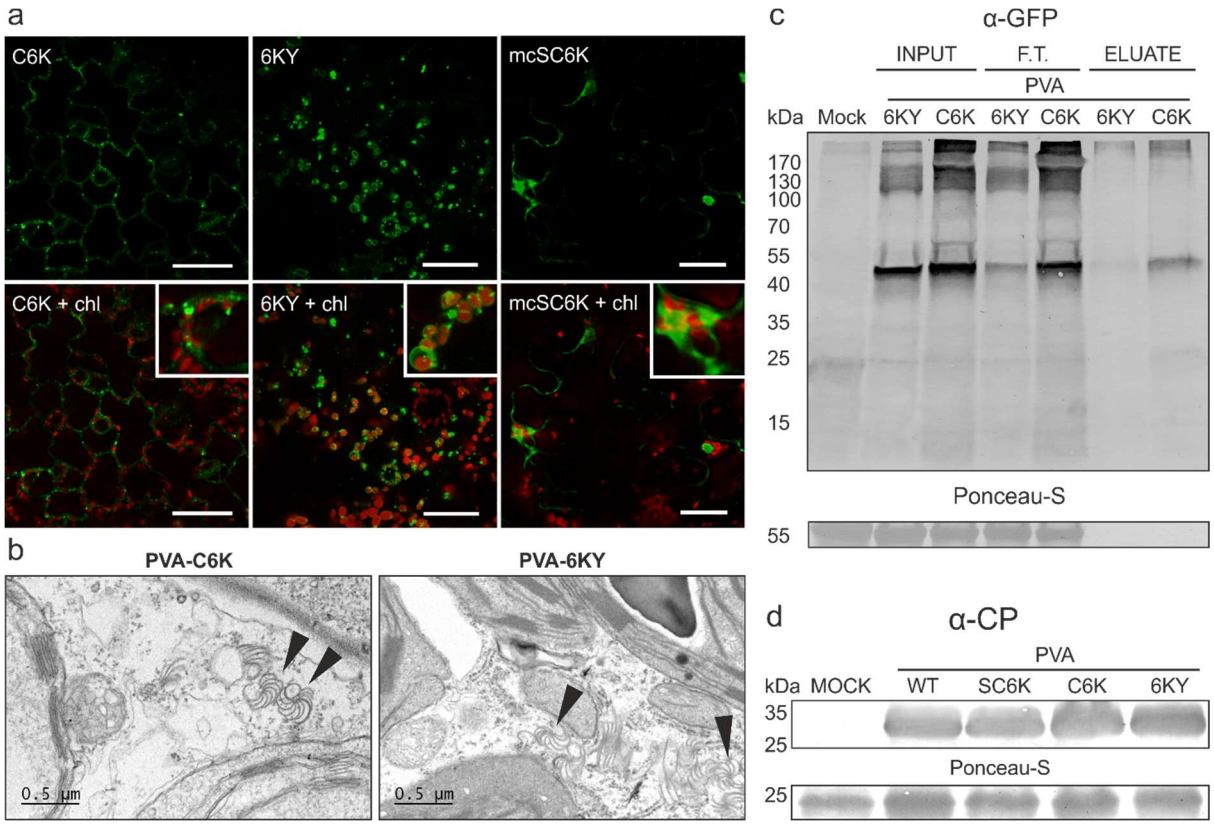
a
C6K
6KY
mcSC6K
C6K + chl
6KY + chl
mcSC6K + chl
b
PVA-C6K
PVA-6KY
0.5 µm
0.5 µm
c
α-GFP
INPUT
F.T.
ELUATE
PVA
kDa Mock 6KY C6K 6KY C6K 6KY C6K
170
130
100
70
55
40
35
25
15
Ponceau-S
55
d
α-CP
PVA
kDa MOCK WT SC6K C6K 6KY
35
25
Ponceau-S
25

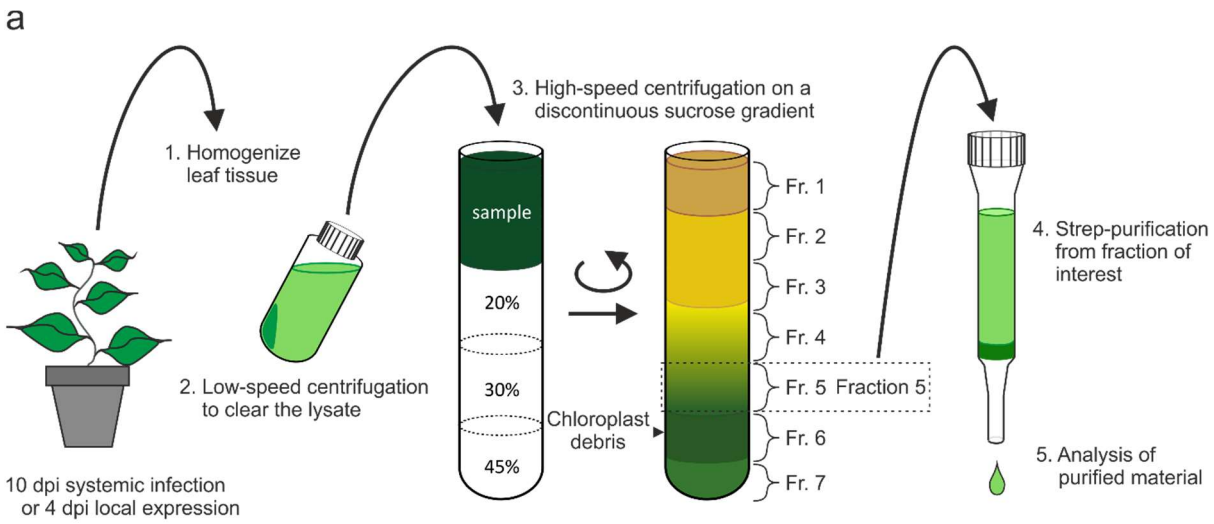
a
1. Homogenize leaf tissue
2. Low-speed centrifugation to clear the lysate
3. High-speed centrifugation on a discontinuous sucrose gradient
sample
20%
30%
45%
Chloroplast debris
Fr. 1
Fr. 2
Fr. 3
Fr. 4
Fr. 5
Fraction 5
Fr. 6
Fr. 7
4. Strep-purification from fraction of interest
5. Analysis of purified material
10 dpi systemic infection or 4 dpi local expression

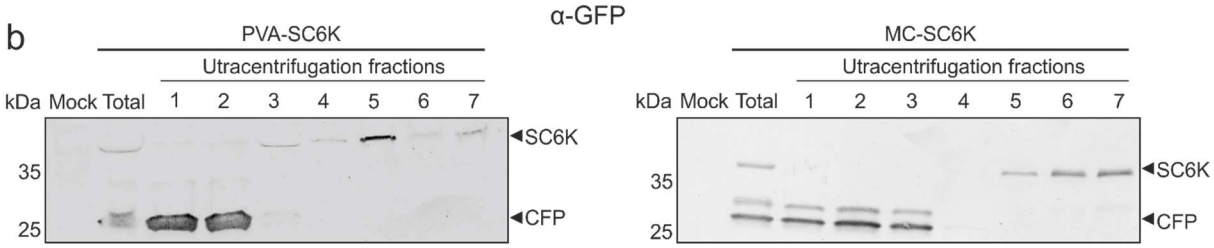
b
α-GFP
PVA-SC6K
Utracentrifugation fractions
kDa Mock Total 1 2 3 4 5 6 7
35
25
SC6K
CFP
MC-SC6K
Utracentrifugation fractions
kDa Mock Total 1 2 3 4 5 6 7
35
25
SC6K
CFP

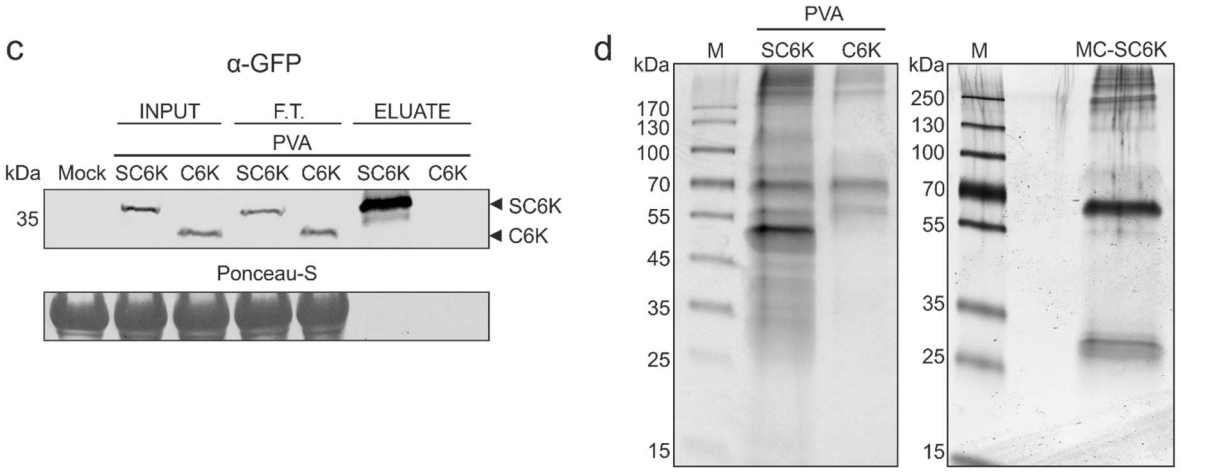
c
α-GFP
INPUT
F.T.
ELUATE
PVA
kDa Mock SC6K C6K SC6K C6K SC6K C6K
35
SC6K
C6K
Ponceau-S
d
PVA
M
SC6K
C6K
kDa
170
130
100
70
55
45
35
25
15
M
MC-SC6K
kDa
250
130
100
70
55
35
25
15

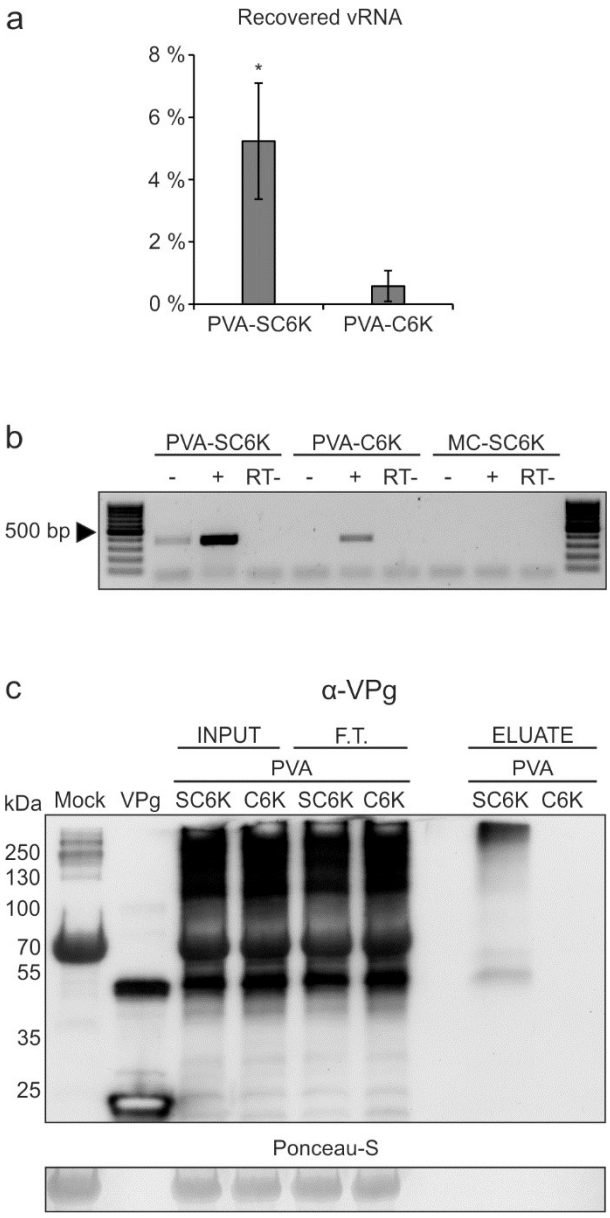
a
Recovered vRNA
8 %
6 %
4 %
2 %
0 %
*
PVA-SC6K
PVA-C6K
b
PVA-SC6K
PVA-C6K
MC-SC6K
- + RT- - + RT- - + RT-
500 bp
c
α-VPg
INPUT
F.T.
ELUATE
PVA
PVA
kDa Mock VPg SC6K C6K SC6K C6K SC6K C6K
250
130
100
70
55
35
25
Ponceau-S

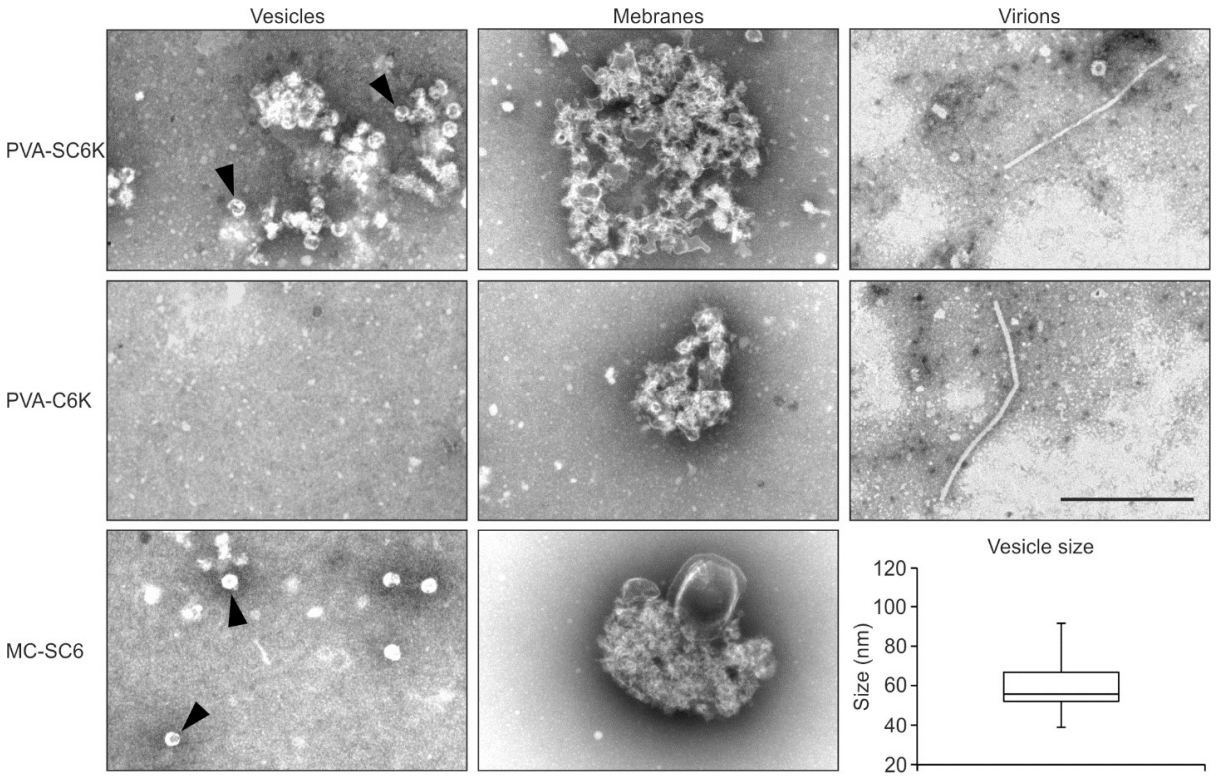
Vesicles
Mebranes
Virions
PVA-SC6K
PVA-C6K
MC-SC6
Vesicle size
Size (nm)
120
100
80
60
40
20